MDPI

Article

CO₂ methanation of biogas over 20 wt% Ni-Mg-Al catalyst: On the effect of N₂, CH₄, and O₂ on CO₂ conversion rate

Danbee Han [1], Yunji Kim [1], Hyunseung Byun [1], Wonjun Cho[2] and Youngsoon Baek [1,*]

[1]   Department of Environmental and Energy Engineering, University of Suwon, Hwaseong-si 18323, Korea; hdbee99 @gmail.com (D.H.); dbswl0547@naver.com (Y.K.),

[2]   Unisys International R&D, Bio Friends Inc., Yuseong-gu, Daejeon 34028, Korea; williamcho86@gmail.com
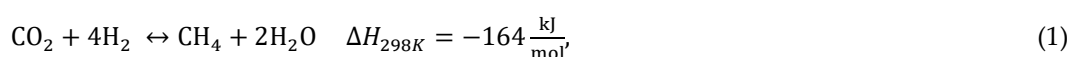
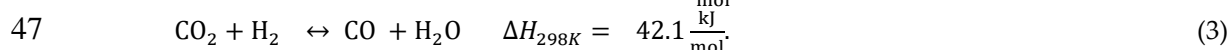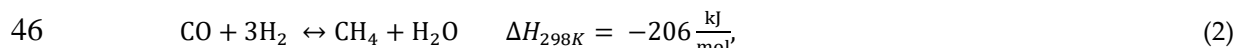*   Correspondence: ysbaek@suwon.ac.kr; Tel.: +82-31-220-2167

Abstract: Biogas contains more than 40% CO_2 that can be removed to produce high quality CH_4. Recently, CH_4 production from CO_2 methanation has been reported in several studies. In this study, CO_2 methanation of biogas was performed over a 20 wt% Ni-Mg-Al catalyst, and the effects of CO_2 conversion rate and CH_4 selectivity were investigated as a function of CH_4, O_2, H_2O, and N_2 compositions of the biogas. At a gas hourly space velocity (GHSV) of 30,000/h, the CO_2 conversion rate was ~79.3% with a CH_4 selectivity of 95%. In addition, the effects of the reaction temperature (200–450 °C), GHSV (21,000–50,000/h), and H_2/CO_2 molar ratio (3–5) on the CO_2 conversion rate and CH_4 selectivity over the 20 wt% Ni-Mg-Al catalyst were evaluated. The characteristics of the catalyst were analyzed using Brunauer-Emmett-Teller (BET) surface area analysis, X-ray diffraction (XRD), X-ray photoelectron spectroscopy (XPS), and scanning electron microscopy (SEM). The catalyst was stable for approximately 200 h at a GHSV of 30,000/h and a reaction temperature of 350 °C. CO_2 conversion and CH_4 selectivity were maintained at 75% and 93%, respectively, and the catalyst was therefore concluded to exhibit stable activity.

Keywords: power to gas; CO_2 methanation; Ni catalyst, biogas utilization, CO_2 hydrogenation

1. Introduction

The recent years have witnessed a growing interest in the regulation of greenhouse gases and the quest for sustainable renewable energy to combat global warming. This has culminated in the demand for an efficient energy storage system (ESS) that can stabilize electric power systems with high output fluctuations. The lithium-ion battery is an ESS widely employed in various energy generation systems owing to its high energy density and efficiency; however, its short shelf life and low storage capacity limit long-term power storage [1]. The availability of organic waste, which is a sustainable energy source, can increase with economic and population growth. Consequently, much attention has been drawn to the utilization of biogas, as it can be easily obtained from livestock (organic) waste and urban solid waste. Biogas, which typically contains 40–65 vol% CH_4, 40–50 vol% CO_2, and minor quantities of (the subsequently removed) N_2, H_2S, O_2, and H_2O [2], is employed as a high-concentration CH_4 fuel after more than 40% of CO_2 is removed using absorbents or amines [3]. The power-to-gas technology generates H_2 from water by employing renewable energy and produces CH_4 via the methanation of H_2 and CO_2. Further, CO_2 methanation and reverse water gas shift (RWGS) are competing processes that occur during the production of CH_4 from CO_2, as described by Equations (1)–(3) [4]. This has become a topic of research considering the possibility of a 'carbon-neutral fuel' and the replacement of natural gas as well as ESSs [5].

$$CO_2 + 4H_2 \leftrightarrow CH_4 + 2H_2O \quad \Delta H_{298K} = -164 \frac{kJ}{mol}, \tag{1}$$

46
$$CO + 3H_2 \leftrightarrow CH_4 + H_2O \qquad \Delta H_{298K} = -206\frac{kJ}{mol},$$
(2)

47
$$CO_2 + H_2 \leftrightarrow CO + H_2O \qquad \Delta H_{298K} = 42.1\frac{kJ}{mol}.$$
(3)

48 Biogas is initially subjected to purification to remove impurities such as H_2S, H_2O, and
49 siloxanes. Subsequently, CO_2 and highly concentrated CH_4 are separated, so that CH_4 can be utilized
50 as fuel [6]. In addition to being used as a fuel, biogas generated by catalytic reforming is also used to
51 produce high-value-added chemicals (e.g., methanol, acetic acid, dimethyl ether, ammonia, and
52 Fischer-Tropsch oil), which greatly contributes to the reduction of greenhouse gas emissions [7,8].
53 Moreover, biogas is an affordable and suitable raw material for syngas production, even though
54 syngas is now largely produced through the CH_4 reforming of natural gas.
55 In a recent study, Mohammad et al. [9] compared the activity of Al_2O_3-supported Ni, Co, Fe,
56 and Mo catalysts during CO_2 methanation. Ni catalyst showed the highest CO_2 conversion and CH_4
57 selectivity, followed by Co, Fe, and Mo. The study by Aziz et al. [10] on the activity of
58 mesostructured silica nanoparticle (MSN)-supported Ni, Fe, and Mo catalysts demonstrated that
59 the Fe catalyst was active at high temperatures, whereas the Ni catalyst exhibited the highest
60 catalytic activity at lower temperatures (<350 °C)[11]. Daroughegi et al. [12] conducted CO_2
61 methanation experiments on Al_2O_3-supported Ni catalysts with different metal loadings, and the
62 results revealed that the specific surface area and CO_2 conversion increased with the increase in the
63 Ni loading from 15, 20, and 25 wt%, whereas the specific surface area and CO_2 conversion
64 decreased at 33 wt%. In the study on Ni/γ-Al_2O_3, Cho et al. [13] reported that the highest dispersion,
65 CH_4 selectivity, and reaction rate were observed at 20 wt% Ni content when the Ni content was
66 varied from 15 to 50 wt%.
67 Jaffar M.M et al. [9] compared the activities of the 10 wt% Ni catalysts supported on SiO_2,
68 MCN, and Al_2O_3. Among the experiments performed at 360 °C, the Ni-Al_2O_3 catalyst showed the
69 highest CO_2 conversion and CH_4 selectivities of 82.9 and 97.9%, respectively. Further, the SEM
70 results confirmed that the Ni particles were more uniformly dispersed in the 10 wt% Ni-Al_2O_3
71 catalyst than those in the 10 wt% MCM and SiO_2 catalysts. It has also been reported that the
72 catalytic activity of SiO_2-supported catalysts for methane production decreases in the presence of
73 H_2O. On MCM, Aziz [14] reported that the CH_4 conversion and selectivity decrease because of the
74 consumption of the carbonyl species by conversion to CO_2 in the presence of water vapor, via the
75 water-gas shift reaction. Vetrivel et al. [15] and Wang et al.[16] reported that the fabrication of the
76 catalysts by reduction on a CeO_2 support generated more surface oxygen vacancies, which resulted
77 in high CO_2 conversion, CH_4 selectivity and enhanced catalyst stability.
78 Typically, promoters are used for improving the activity of supported catalysts. For example,
79 the promoter MgO can increase carbon resistance [17]**,** thermal stability **[18],** and the dispersion of
80 Ni/Al_2O_3 catalysts [19,20], affording enhanced activity [21,22]. Thus, MgO, in combination with
81 support materials such as Al_2O_3 or SiO_2 has been proposed as a support for methanation catalysts
82 [23,24]. Bette et al. [25] demonstrated that the maximum CO_2 conversion of 74% was obtained with
83 a 59 wt% Ni/(Mg,Al)O_x catalyst, and the addition of MgO to Ni/SiO_2 resulted in a conversion of 66.5%
84 [14]. In addition, MgO is a basic material that absorbs carbon dioxide and reduces catalyst
85 deactivation via sintering and carbon deposition [26]. While catalysts become inactive because of
86 the water produced during CO_2 methanation, MgO reacts with water to generate magnesium
87 peroxide (Mg(OH)$_2$) and thereby mitigates catalyst deactivation [27,28].
88 The activation energy of Ni catalysts for methanation was 93.61 kJ/mol in Ni/ZrO_2 catalysts
89 [29], 75 kJ/mol in Ni/Al_2O_3 catalysts [30], and 75 kJ/mol in Ni/Al hydrotalcite catalysts [31].
90 The present work studies the production of CH_4 by the reaction of biogas CO_2 with hydrogen
91 over a 20 wt% Ni-Mg-Al catalyst and characterizes this catalyst by several instrumental analyses.
92 The conditions for the reaction of biogas, including reaction temperature, space velocity, and
93 H_2/CO_2 ratio, were varied to investigate their effects on CO_2 conversion, CH_4 yield, and selectivity.
94 In addition, because biogas is a mixture of various gases and trace elements, the effect of the
95 concentration of these components (N_2, O_2, CH_4, and CO_2) on CO_2 conversion, CH_4 yield, and
96 selectivity were studied. Based on this, the optimal reaction conditions for producing CH_4 from

97 biogas were determined, under which a stability test of the 20 wt% Ni-Mg-Al catalyst was
98 performed for 200 h.

99 **2. Materials and Methods**

100 *2.1 Catalyst preparation*

101 The catalyst used in this study is a 20 wt% Ni-Mg-Al catalyst (supported by Korea Institute of
102 Energy Research). The catalyst was prepared on a Ni metal that exhibits high catalytic activity and
103 CH_4 selectivity. The catalyst was prepared by mixing calculated ratios of $Ni(NO_3)_2 \cdot 6H_2O$,
104 $Al(NO_3)_2 \cdot 9H_2O$, and $Mg(NO_3)_2 \cdot 6H_2O$ solutions at 60 °C until the Ni content was 20, 40 wt%, and
105 a precipitate was obtained after adding a precipitant to the mixture and stirring for approximately 1
106 hour while maintaining a constant pH. The precipitated catalyst precursor was repeatedly washed
107 with distilled water and filtered with a filter press until the pH reached approximately 7.0. The
108 catalyst precursor was then dried in an oven at 150 °C for 12 h, and 20/40 wt% $Ni-Mg-Al_2O_3$
109 catalysts were prepared through a heat treatment process under an air atmosphere at 600 °C for 4 h.
110 Prior to their use, all catalysts were heated to the reduction temperature under a gas flow of 100
111 ml/min (20% H_2, 80% N_2) for 2 h, and the catalysts were reduced while the temperature was
112 maintained for 4 h.
113 Figure 1 illustrates the variations in catalytic activity of the 40 wt% $Ni-Mg-Al_2O_3$ catalysts at
114 the reaction temperatures of 350 and 400 °C as a function of changes in the reduction temperatures
115 to 450, 550, 700, and 800 °C. The CO_2 conversion initially showed a significant increase as the
116 reduction temperature increased, while the CO_2 conversions at 700 and 800 °C were similar;
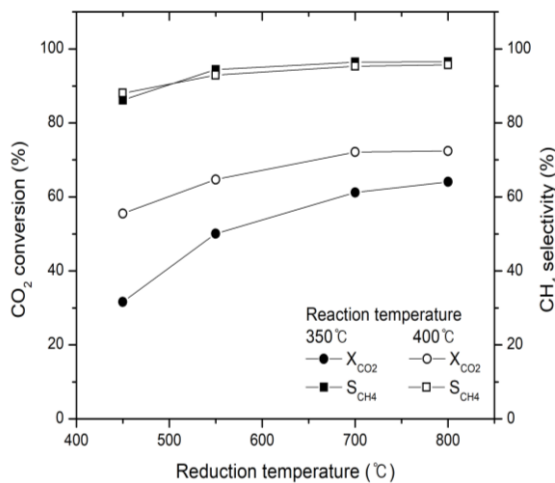117 therefore, 700 °C was used as the reduction temperature of the catalysts.

118

119 **Figure 1.** Effect of reduction temperature on CO_2 conversion and CH_4 selectivity over the 40 wt%
120 Ni-Mg-Al catalyst.

121 *2.2 CO_2 methanation apparatus and activity test*

122 Isothermal CO_2 methanation experiments were conducted in a plug-flow system (Figure 2) at
123 steady state with Ni catalysts loaded into the reactor. The catalytic reactor has an outer diameter of
124 12.7 mm (1/2"), a thickness of 1.257 mm, a length of 209 mm, and Inconel 800HT composed of 80%
125 Ni, 14% Cr, and 6% Fe. During the experimentation, a mesh sieve was installed in the lower part of
126 the reactor to support the catalyst layer, and 0.5 g of the catalyst was loaded. A back-pressure
127 regulator (BPR) in the latter section of the reactor was used to control the reaction pressure from 1
128 to 9 atm. A water trap in the latter section of the BPR was used to remove the water generated from
129 the reaction, and a high-pressure check valve was installed to prevent gas backflow. All tubes used
130 were of SUS grade with an outer diameter of Φ3.2 mm and thickness of 0.8 t, and the products were

131 analyzed using gas chromatography (GC). To prevent the condensation of the products inside the
132 tube during this process, a line heater was installed and maintained above 150 °C.
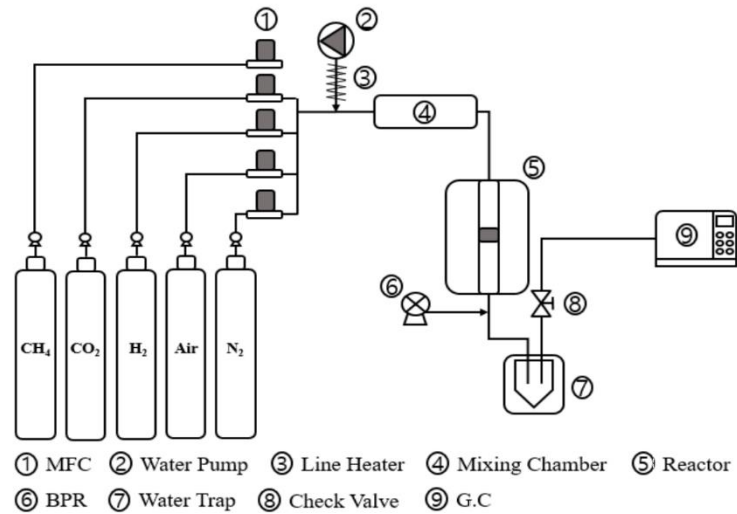

Figure 2. Schematic of CO_2 methanation.

133   The reaction products were characterized using a GC (YL Instrument 6500), SS COL 10FT 1/8"
134 PORAPACK N (Model: 13052-U) and Phase None Matrix 45/60 Molecular Sieve 13X were used for
135 the GC columns, and argon was used as the carrier gas. Hydrogen, methane, and carbon monoxide
136 were analyzed with a thermal conductivity detector (TCD), whereas carbon dioxide was analyzed
137 using a flame ionization detector (FID). Characterization in the GC oven was conducted by
138 maintaining the temperature initially at 35 °C for 0–6 min and raising it to approximately 170 °C at
139 a ramp rate of 15 °C /min. FID characterization was performed at 250 °C by supplying 35 ml/min of
140 hydrogen and 300 ml/min of oxygen, while TCD characterization was carried out at 150 °C under a
141 gas flow rate of 35 ml/min of hydrogen and 20 ml/min of Ar. CO_2 conversion (X_{CO2}), CH_4 selectivity
142 (S_{CH4}), and CH_4 yield (Y_{CH4}) were calculated according to Equations (4)–(6)[32].

$$X_{CO2} \ (\%) = (1 - \frac{CO_2}{CH_4 + CO + CO_2}) \times 100, \qquad (4)$$

$$S_{CH4} \ (\%) = (\frac{CH_4}{CH_4 + CO}) \times 100, \qquad (5)$$

$$Y_{CH4} \ (\%) = \frac{X_{CO2} \times S_{CH4}}{100}. \qquad (6)$$

146   Using a reactant gas flow rate of 250 ml/min, reaction temperature of 350 °C, GHSV of 30,000/h,
147 and H_2/CO_2 ratio of 4 as the basis, methanation reaction experiments were conducted by changing
148 the experimental conditions, as listed in Table 1.

149   **Table 1.** Experimental condition for CO_2 methanation reaction.

	Items	Condition	Remark
	Reaction Temperature (°C)	200–450	
	CH_4 and CO_2 composition ratio (%)	65:35, 50:50, 40:60	
Variable	GHSV (/h)	21,000–50,000	
	H_2/CO_2 mole ratio	3.5, 4, 4.5, 5	
	O_2 (cc/min)	10.5 (4%)	

150 *2.3. Catalyst characterization*

151 2.3.1 Brunauer-Emmett-Teller (BET) measurement

152   The BET specific surface area, which is one of the key catalyst properties, was measured using
153 ASAP 2020 Plus Physisorption(Center for advanced materials analysis, Suwon University). A

154 known amount of catalyst sample was added to the BET measurement tube, and the moisture in the
155 catalyst was removed through a pretreatment process under a vacuum of 10 μm Hg by heating to
156 250 °C at a ramp rate of 10 °C/min for 12 h, after which the weight of the catalyst sample was
157 measured.
158   Measurements of the specific surface area, pore-volume, and pore size of the fresh (20 and 40
159 wt% Ni-Mg-Al) and spent (20 wt% Ni-Mg-Al catalyst after 200 h of use) catalysts are summarized
160 in Table 2. The BET surface area of the spent catalyst decreased in comparison with that of the fresh
161 catalyst. In addition, an increase in the Ni content led to a decrease in the specific surface area, which
162 is attributed to the blocking of catalyst pores with increasing Ni content, similar to the results
163 reported by Daroughegi et al. [12] with catalysts containing greater than 20 wt% of Ni. In addition,
164 these observations were similar to the results obtained by A. Zhao et al. [33]—the Ni metal crystal
165 size increased in the catalysts comprising Ni loadings greater than 20 wt%. For this reason, the 20
166 wt% catalyst showed a higher CO_2 conversion than the 40 wt% catalyst (Table 3).

167   **Table 2.** Brunauer-Emmett-Teller (BET) surface area, pore volume, and pore size of 20 wt%
168   Ni-Mg-Al catalyst (fresh and spent).

Catalyst		BET(m^2/g)	Total pore volume (m^3/g)	Pore size (Å)
20 wt% Ni-Mg-Al	Fresh	180.33	0.36	81.530
	spent	148.9	0.3	81.15
40 wt% Ni-Mg-Al	Fresh	152.61	0.31	82.13

169

170   **Table 3.** CO_2 conversion & selectivity of CH_4 with different Ni loadings.

Catalyst	Reaction temperature (°e)	CO_2 conversion (X_{CO2})	CH_4 selectivity (S_{CH4})
20 wt% Ni-Mg-Al	350	75.0	94.2
	400	75.6	93.0
40 wt% Ni-Mg-Al	350	61.2	96.4
	400	72.2	95.3

171
172 2.3.2 X-ray diffraction (XRD) characterization
173   The elemental composition of the catalysts was characterized using an XRD diffractometer
174 (ThermoFisher Scientific, ARL Equinox 3000(Center for advanced materials analysis, Suwon
175 University). The catalyst powder samples were pretreated at 250 °C for 5 h to remove moisture, and
176 the crystals of the catalysts were analyzed. Cu-Kα radiation was used to fix the axis of the sample,
177 and measurements were performed at 30 mA and 40 kV over a 2θ range 10–80° using a scanning
178 speed of 8θ/min. The XRD analysis results of the catalytic supports and Ni catalysts before and after
179 the reaction are shown in Figure 3. Diffraction peaks that appear at 2θ values of 37.3°, 43.3°, 62.9°,
180 and 75.4° are associated with the NiO phase, whereas those at 44.55°, 51.85°, and 76.3° are
181 associated with Ni metal. The 2θ values of 45.86 and 66.91 correspond to MgO, whereas the
182 diffraction peaks at 2θ values of 37.4°, 46.07°, and 66.9° are associated with the alumina phase.
183 Figure 3 shows the XRD characterization of the catalysts before and after reduction at 700 °C and on
184 the spent catalyst 200 h after the reaction. As shown in the figure, peaks corresponding to Ni metal
185 were not observed in the fresh catalyst prior to the reaction, whereas NiO peaks were observed[34].
186 In contrast, the reduction catalyst and spent catalyst exhibited prominent Ni metal peaks at 2θ
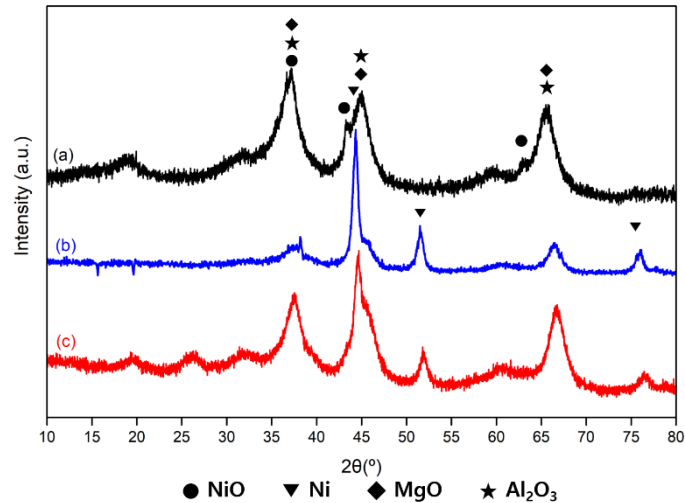187 values of 51.85° and 76.3°, respectively [30].

Figure 3. X-ray diffraction patterns of (**a**) fresh, (**b**) reduced at 700 °C in the fresh state, and (**c**) spent 20 wt% Ni-Mg-Al catalysts.

2.3.3 H_2-TPR analysis

The interaction and reduction between the catalyst metal and support were characterized by H_2-temperature-programmed reduction (H_2-TPR). As shown in Figure 4, the H_2 consumption of the catalysts appeared between 300, 400, and 450–1,000 °C. The two peaks correspond to the reduction of the NiO particles. The first peak refers to the reduction of NiO particles that exhibit a weak interaction due to MgO, and the second peak that appears at high temperatures corresponds to the reduction of NiO. Al_2O_3 particles with spinel structures that exhibit a strong interaction between the NiO particles and the Al_2O_3 support. An improved H_2 consumption was observed as the Ni content of the catalysts increased.
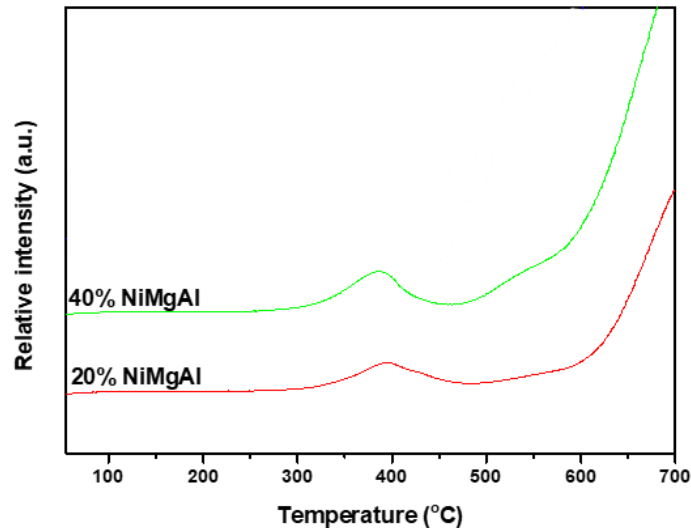

Figure 4. Hydrogen temperature-programmed desorption profiles of 20, 40, and 60 wt% Ni-Mg-Al catalysts.

2.3.4 XPS characterization

To investigate the oxidation state of the catalysts, X-ray photoelectron spectroscopy (XPS, K-Alpha plus, Thermo Scientific, Center for advanced materials analysis, Suwon University) was used to measure the binding energy. XPS characterization was performed under vacuum using Al-Kα radiation on a fresh catalyst and on the spent catalyst after 200 h of reaction, without any separate sample pretreatment process (Figure 5). The oxidation state of Ni can be determined from

210   the binding energy (BE) of the XPS Ni2p3/2 spectrum. The Ni2p3/2 BE of NiO is 855–856 eV, and
211   that of the Ni metal is 852.3–852.6 eV[35]. As shown in the figure, the XPS spectrum for the BE of
212   the fresh catalyst displayed peaks 854.9 and 855.7 eV that are associated with NiO (peaks at 853.4
213   and 855.3 eV), and a small amount of Ni(OH)$_2$ (peaks at 861.5 eV). The XPS pattern of the spent
214   catalyst revealed the presence of Ni metal near 851.8 eV in addition to NiO and Ni(OH)$_2$.
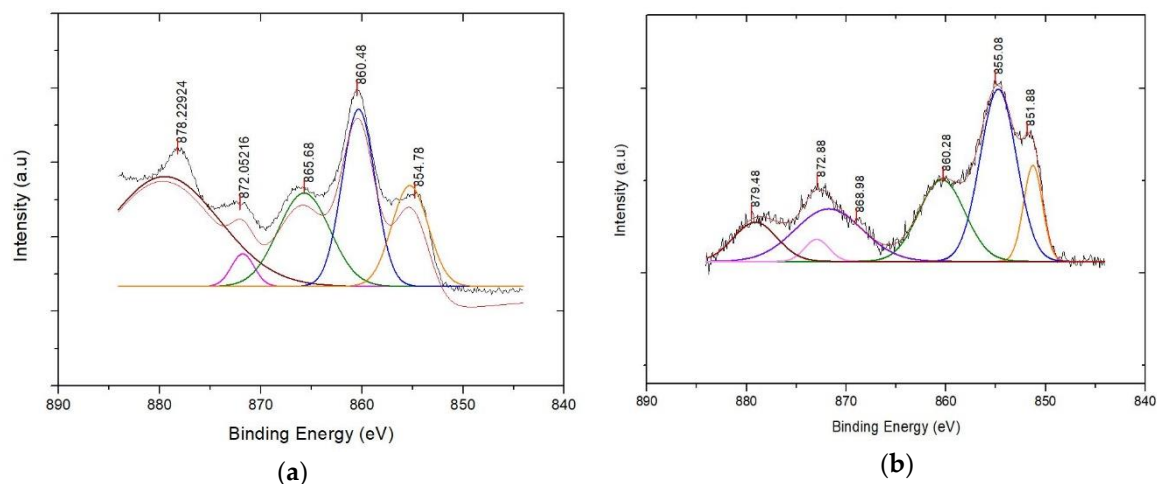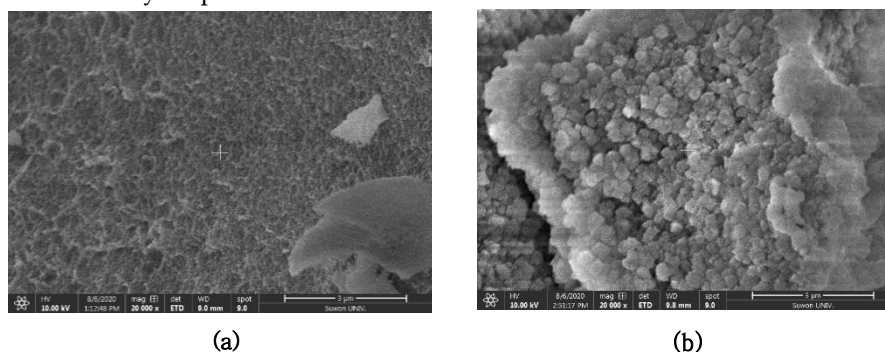

(**a**)   (**b**)

215   **Figure 5.** X-ray photoelectron spectra of (**a**) fresh and (**b**) spent 20 wt% Ni-Mg-Al catalysts.

216   2.3.5 Scanning electron microscopy (SEM)–energy-dispersive X-ray spectroscopy (EDX)
217   characterization

218   SEM-EDX was used to investigate the surface morphology of the catalysts and the dispersion
219   of Ni. FEI APREO SEM(Center for advanced materials analysis, Suwon University) was used to
220   obtain images at 20,000 × magnification of the catalyst samples prepared by removing powders and
221   dust, drying at 120 °C for 1 h, and coating with metal (Au). SEM images of the fresh catalyst and the
222   spent catalyst after 420 h of reaction are presented in Figure 6. As shown in the SEM images,
223   nanoscale particles were uniformly dispersed throughout the surface. Owing to the decomposition
224   of Mg(NO$_3$)$_2$·6H$_2$O to MgO at temperatures above 600 °C, it was confirmed that spherical [36]
225   particles were uniformly dispersed.
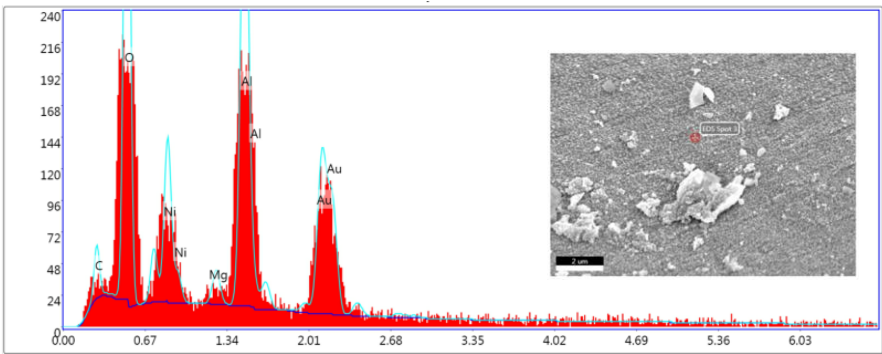

(a)   (b)

Figure 7. Scanning electron microscopy–energy-dispersive X-ray spectroscopy analysis of 20 wt% Ni-Mg-Al catalyst.

226   **Figure 6.** Scanning electron microscopy images of (**a**) fresh and (**b**) spent 20 wt% Ni-Mg-Al catalysts.

227   The results of the elemental composition analysis of the catalyst using EDX and of the surface
228   morphology characterization from the SEM image are shown in Figure 7. The contents of Ni, Mg,
229   and Al metals from the cross-section of the catalysts are summarized in Table 4.

230   **Table 4.** Elemental composition of 20 wt% Ni-Mg-Al catalyst determined by scanning electron
231   microscopy–energy-dispersive X-ray spectroscopy.

Element	C	O	Ni	Mg	Al
Weight (%)	4.82	36.99	16.80	2.59	38.80

232

233   **3. Results and Discussion**

234   *3.1 Effect of reaction temperature on CO_2 conversion*

235   The dependence of CO_2 conversion and CH_4 selectivity on reaction temperature at a GHSV of
236   30,000/h and H_2/CO_2 ratio of 4 is displayed in Figure 8. As shown in the figure, CO_2 conversion
237   increased as the temperature increased and reached a maximum at 400 °C, whereas CH_4 selectivity
238   and yield showed the highest values at 350 °C. This trend is probably the result of CO_2 methanation
239   suppression above 350 °C, whereas the RWGS reaction is enhanced, which resulted in the
240   conversion of CO_2 to CO. This result was confirmed in a study by Mohammad et al. [9], in which
241   the CO concentration increased as the RWGS reaction increased at 400 °C, whereas the methane
242   selectivity decreased. A study by Jia et al. [29] also reported that the highest CO_2 conversion and
243   CH_4 yield were observed at 350 °C as the temperature increased, and a further increase in
244   temperature decreased the CO_2 conversion because of the thermodynamic equilibrium limit [37].
245   In addition, the activation energy obtained from the 20 wt% Ni-Mg-Al catalyst was
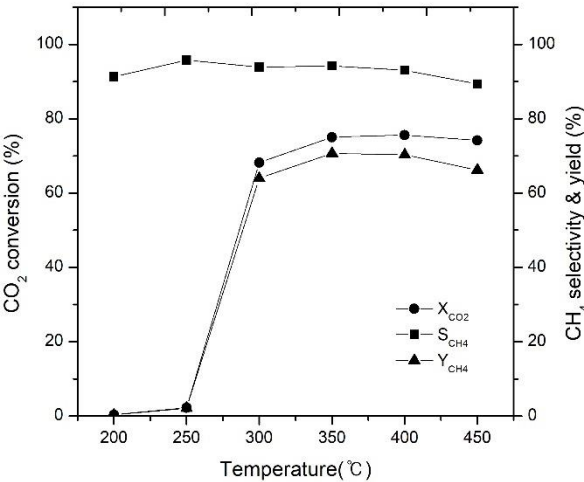

Figure 8. Effect of reaction temperature.

246 approximately 74.2 kJ/mol, which was similar to the 75 kJ/mol obtained as the value with the use of
247 Ni/Al_2O_3 in the study by Carbarino [30].

248 *3.2 Effect of H_2/CO_2 ratio on CO_2 conversion*

249   Figure 9 shows the effects of the H_2/CO_2 ratio at a reaction temperature of 350 °C and a GHSV
250 of 30,000/h on CO_2 conversion and CH_4 selectivity/yield. Figure 9(a) shows the results obtained for
251 different H_2/CO_2 ratios by increasing the amount of H_2 at a given amount of CO_2 and by increasing
252 the amount of CO_2 at a given amount of H_2. Figure 9(b) shows the effects of increasing the reactant
253 amounts at a given H_2/CO_2 ratio. As shown in Figure 9(a), the CO_2 conversion and CH_4 yield
254 increased by approximately 15% when the ratio of H_2 increased from 3.5 to 5, whereas the CH_4
255 selectivity remained almost constant. As shown in Figure 9(b), the same H_2/CO_2 ratio led to similar
256 CO_2 conversion and CH_4 selectivity and yield, regardless of the amount of reactants. These results
257 were similar to those from a study by Rahmani [38] in which a 15% increase was observed when the
258 H_2/CO_2 ratio was increased from 3 to 4, and the study by Aziz et al. [39] also reported that the
259 concentration of hydrogen affects the catalytic activity because of hydrogen adsorption onto the
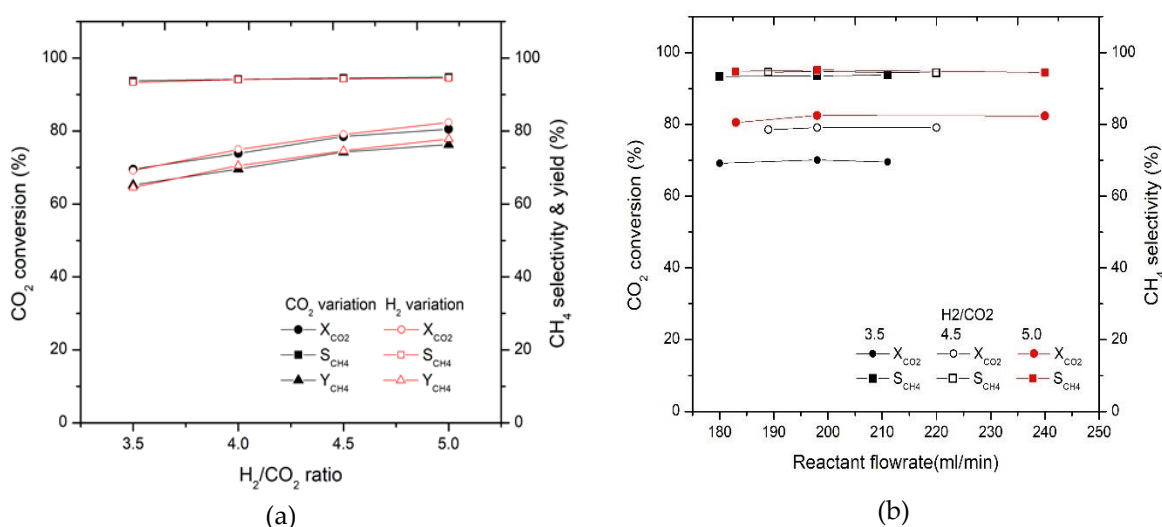260 surface of the catalyst and the conversion to methane via hydrogenation.

(a)   (b)

261   **Figure 9.** Effect of H_2/CO_2 mole ratio along with (**a**) CO_2 or H_2 variation; (**b**) reactant amount
262   variation.

263 *3.3 Effect of GHSV on CO_2 conversion*

264   The effects of increasing GHSV on CO_2 conversion and CH_4 selectivity and yield at a reaction
265 temperature of 350 °C and H_2/CO_2 ratio of 4 are shown in Figure 10(a) and (b). The effect of
266 increasing the reactant flow rate to change the GHSV to 21,000–50,000/h is shown in Figure 10(a),
267 and the effect of increasing the amount of nitrogen at a given reactant flow rate to change the GHSV
268 to 9,000–38,000/h is shown in Figure 10(b). As shown in the figure, CO_2 conversion and CH_4
269 yield/selectivity showed a general decreasing trend as the GHSV increased, and the effect for (b)
270 was larger than that for (a). This is because an increase in GHSV shortens the time during which the
271 reactants CO_2 and H_2 are in contact with the catalyst, thus reducing the amount of reactants
272 adsorbed onto the surface of the catalyst. These results were consistent with the experimental
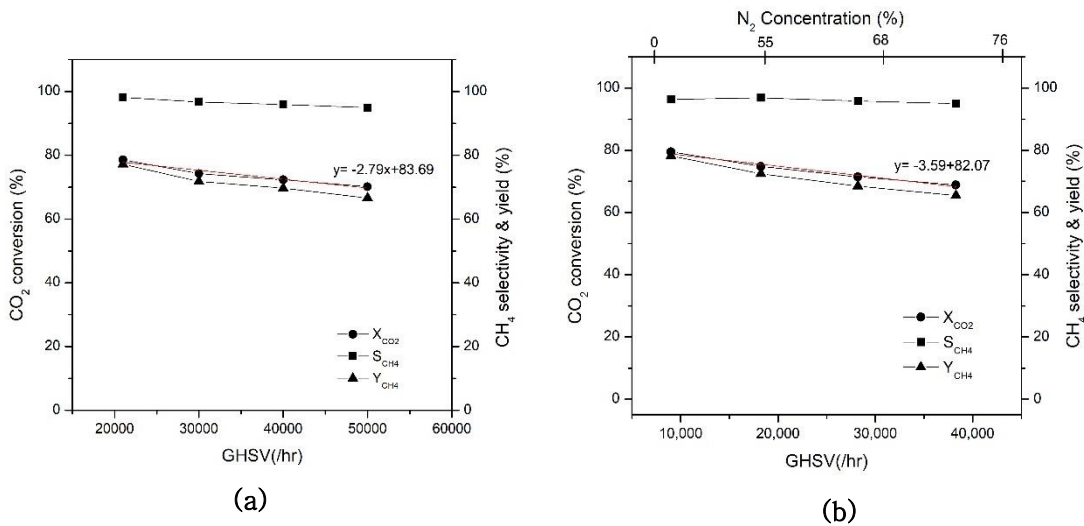273 results reported by Abate et al. [40]

(a)   (b)

Figure 10. Effect of increased gas hourly space velocity & N_2 concentration at H_2/CO_2 ratio of 4 and reaction temperature of 350 °C (**a**) total reactant flow rate (**b**) N_2 flow rate (N_2 concentration).

3.4 Effect of initial concentration of biogas components on CO_2 conversion

3.4.1 Effect of initial CH_4 concentration on CO_2 conversion

The effect of changing the initial CH_4 concentration to 0, 50, and 65 vol% for CO_2 conversion at a reaction temperature of 400 °C, GHSV of 30,000/h, and H_2/CO_2 ratio of 4 is shown in Figure 11. As shown in the figure, increasing the content of CH_4 in the reactant gas to 40, 50, and 65 vol% led to low CO_2 conversions of approximately 67, 64, and 54%, respectively, resulting in up to a 20% decrease in the CO_2 conversion compared to that in the absence of CH_4. This phenomenon is attributed to the Le Chatelier principle, in which the initial CH_4 present in the reactant gas inhibits the conversion to CH_4. These results were also reported in a simulation study by Jurgensen [41], wherein CO_2 conversion decreased as the initial methane concentration increased.
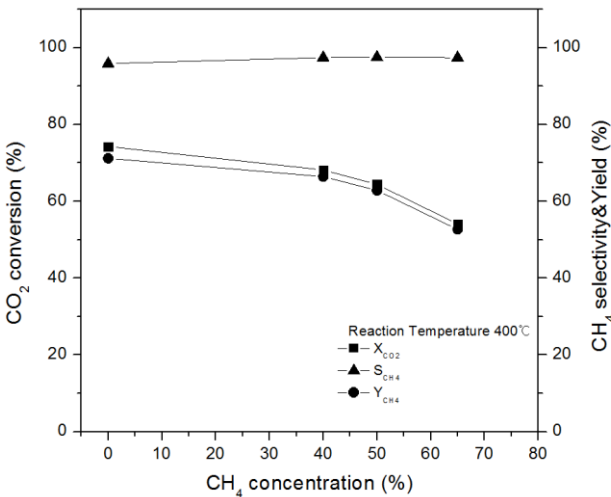

Figure 11. Effect of biogas composition ($CH_4:CO_2$ = 65:35, 50:50).

3.4.2 Effect of initial CO_2 concentration on CO_2 conversion

The effect of increasing the initial CO_2 concentration on CO_2 conversion and CH_4 selectivity at a reaction temperature of 350 °C, GHSV of 30,000/h, and H_2/CO_2 ratio of 4 are presented in Figure 12. As shown in the figure, an increase of CO_2 in biogas from 10 to 14 vol% at a GHSV of 30,000/h resulted in a 2% increase in CO_2 conversion and a 3% increase at a GHSV of 50,000/h. This is

292   probably due to the increase in reaction temperature from the exothermic reaction of CO_2
293   methanation with increasing amounts of the reactants, such that the increase in CO_2 conversion is
294   greater at a GHSV of 50,000/h than at 30,000/h, because more reactants are present in the former
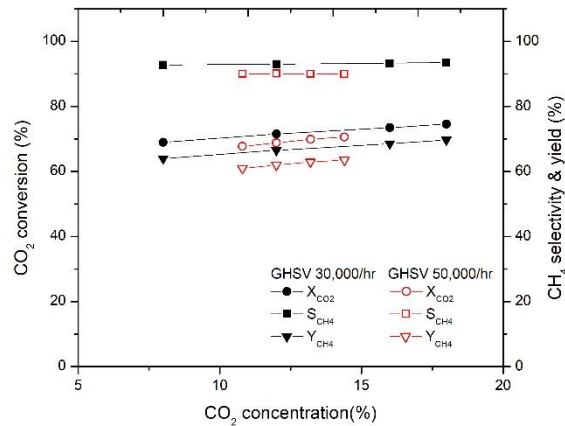295   case than in the latter.

296

297   **Figure 12.** Effect of reactant concentration [= $CO_2/(H_2+CO_2+N_2)$] at a reaction temperature of 350 °C.

298

299   3.4.3 Effect of initial N_2 concentration on CO_2 conversion

300   Approximately 15% of N_2 exists in landfill gas—a type of biogas—and is used as an inactive
301   gas to prevent the deactivation of catalysts caused by the spot exothermic reaction of CO_2
302   methanation. The effect of the presence of 0, 10, and 30% N_2 in the reactant gas on CO_2 conversion
303   at a GHSV of 15,000/h and H_2/CO_2 ratio of 4 is shown in Figure 13. When nitrogen concentrations
304   were 10 and 30% in the reactant, the respective CO_2 conversions were approximately 3 and 5%
305   lower than that in the absence of N_2. This is believed to be due to the decrease in reactant
306   concentration as the N_2 concentration increases, resulting in less heat generation, which, in turn,
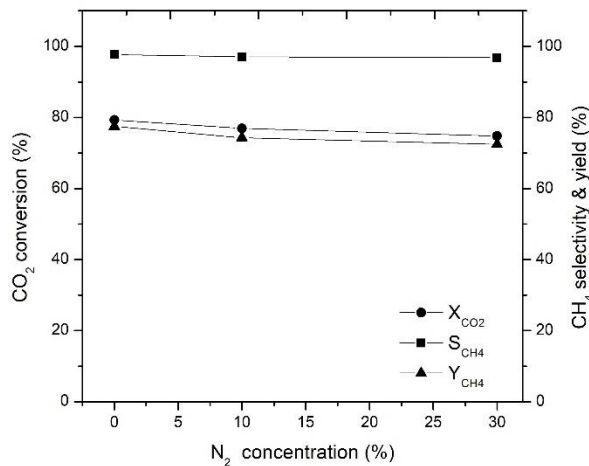307   lowers the reaction temperature.

308

309   **Figure 13.** Effect of N_2 in biogas at reaction temperature of 350 °C.

310   3.4.4 Effect of initial oxygen concentration on CO_2 conversion

311   The effects of the presence of oxygen in the reactant gas on CO_2 conversion at a GHSV of
312   30,000/h, an H_2/CO_2 ratio of 4, and reaction temperatures of 300 and 400 °C are shown in Figure 14.
313   When 4% oxygen was present in the reactant gas, CO_2 conversion and selectivity decreased by
314   approximately 5 and 3%, respectively. This is thought to be a protected re-oxidation reaction due to
315   the presence of oxygen in the reactant gas, which prevents the forward reaction in CH_4 synthesis
316   paths (1) and (2). According to the mechanism proposed by Lin et al. [21], CO_2 is separated from the
317   oxygen vacancies on the Ni metal and support material, which are produced during the reduction
318   of catalysts, and it is reported that a decrease in the oxygen vacancies on the catalyst and support
319   reduces the catalytic activity. Therefore, it is considered that the CO_2 conversion and selectivity
320   decrease in the presence of oxygen because of the decrease in the amount of oxygen vacancies on
321   the Ni catalyst and support, which prevents CO_2 from being converted to CO or carbon species, or
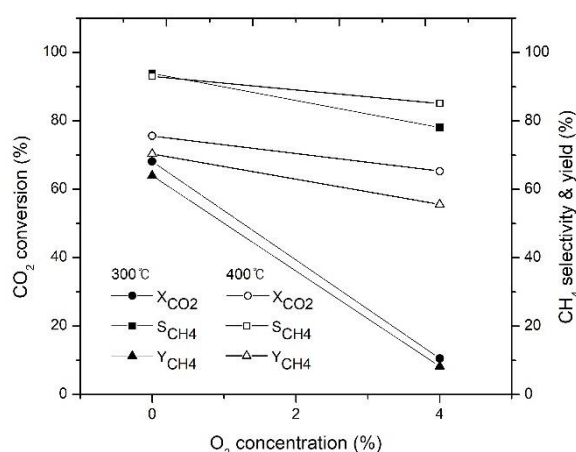322   because of the re-oxidation of CO.

Figure 14. Effect of O_2 in reaction gas.

323   *3.5 Stability and activity of catalyst test*

324   To evaluate the activity and stability of the catalysts, CO_2 methanation was conducted at a
325   GHSV of 30,000/h, reaction temperature of 350 °C, and H_2/CO_2 ratio of 4 for 200 h. As shown in
326   Figure 15, the CO_2 conversion was constant at 75%, and CH_4 selectivity was 93% for 200 h. These
327   results confirmed the activity and stability of the 20 wt% Ni-Mg-Al catalyst for the CO_2
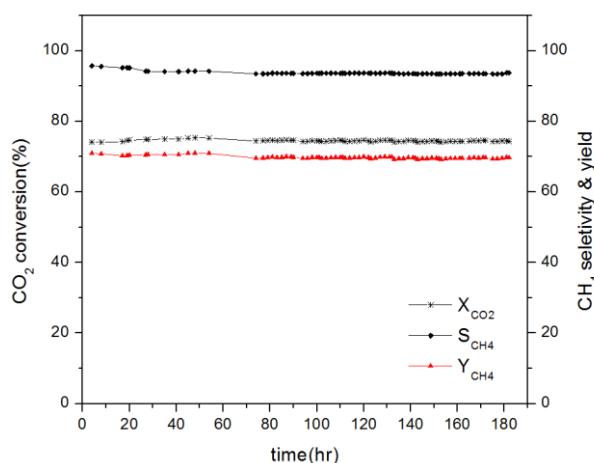328   methanation reaction.

Figure 15. Stability test over 20 wt% Ni-Mg-Al catalysts at reaction temperature of 350 °C, a gas
hourly space velocity of 30,000/h, and a H_2/CO_2 ratio of 4.

4. Conclusion

In this study, the reaction between H_2 and the CO_2 present in biogas was explored, and the experiments on CO_2 methanation for producing CH_4 were conducted over a 20 wt% Ni-Mg-Al catalyst. The optimal conditions for CO_2 methanation over the 20 wt% Ni-Mg-Al catalyst were determined based on the effects of the reaction temperature, GHSV, and H_2/CO_2 ratio on CO_2 conversion. Furthermore, experiments investigating the effects of CO_2, CH_4, N_2, and O_2 concentrations (i.e., biogas composition) on CO_2 conversion led to the following conclusions.

1) CO_2 conversion increased as the reaction temperature increased, but decreased beyond 400 °C, and the highest values of CH_4 selectivity and yield were obtained near 350 °C. This is due to the thermodynamic equilibrium limit that reduces the CO_2 conversion at temperatures above 400 °C [29] and inhibits the methanation reaction above 350 °C via the RWGS reaction, which increases the production of CO and decreases the CH_4 selectivity. The activation energy at this point was 72.4 kJ/mol.

2) CO_2 conversion and CH_4 selectivity increased as the H_2/CO_2 ratio increased from 3.5 to 5.0, whereas the CO_2 conversion resulted in similar values as long as the H_2/CO_2 ratio remained the same regardless of the H_2 and CO_2 concentrations when the H_2/CO_2 ratio was varied. Increasing the GHSV of the reactant gas and its N_2 concentration shortened the contact time between the reactant and catalyst and reduced the CO_2 conversion.

3) A higher initial concentration of CO_2 in the biogas led to a slightly higher CO_2 conversion, but increasing the initial CH_4 concentration to 40, 50, and 65 vol% decreases the CO_2 conversion by up to 20% compared to that in the absence of CH_4. This trend is believed to be the result of Le Chatelier's principle, in which the conversion of CH_4 was suppressed by the initial concentration of CH_4 in the reactant gas. The selectivity was shown to be independent of CH_4 concentration and remained constant.

4) Investigation of the effect of the concentrations of N_2 and O_2 components of biogas revealed that CO_2 conversion decreased by approximately 5% in the presence of 10 vol% N_2. In the presence of O_2, the CO_2 conversion decreased as a result of the decrease in the number of active sites of the Ni catalyst due to oxygen, which also reduced the CH_4 selectivity because of the re-oxidation reaction.

5) The stability of the 20 wt% Ni-Mg-Al catalyst for CO_2 methanation was evaluated from experiments at 350 °C for 200 h. The catalyst is expected to exhibit stable activity, because the CO_2 conversion and CH_4 selectivity were maintained at constant values of 75 and 93%, respectively.

In future, we plan to (i) apply the developed strategy to power plants (which generate much CO_2) and food waste treatment plants (which generate much anaerobic digestion gas) to produce methane gas and (ii) carry out demonstration tests for use in natural gas grids and natural gas–powered vehicles.

References

1. Lee, S.H. The Role of Hydrogen Energy for Renewable Energy 3020, KDB Research, Vol. 749, 2018.

2. Nam, J.J.; Shin, J.D.; Hong, S.G.; Hahm, H.S.; Park, W.K.; So, K.H. Biomethanol conversion from biogas produced by anaerobic digestion. *J. Korea Org. Resour. Recycl. Assoc.* **2006**, *14*, 93–103.

3. Petersson, A.; Wellinger, A. Biogas upgrading technologies – Developments and innovations. IEA Bioenergy Report, 2009.

4. Li, W.; Wang, H.; Jiang, Z.; Zhu, J.; Liu, Z.; Guo, X.; Song, C. A short review of recent advances in CO_2 hydrogenation to hydrocarbons over heterogeneous catalysts. *RSC Adv.* **2018**, *8*, 7651–7669.

5. Shayan, E.; Zare, V.; Mirzaee, I. Hydrogen production from biomass gasification; a theoretical comparison of using different gasification agents. *Energy Convers. Manage*. **2018**, *159*, 30–41.

6. Sternberg, A.; Jensa, C.M.; Bardow, A. Life cycle assessment of CO_2-based C1-chemicals. *Green Chem.* **2017**, *19*, 2244–2259.

7. Jessica L. E.; Kovarik, L.; Kenvina, C.K.; Sievers, C. Effect of preparation methods on the performance of Co/Al_2O_3 catalysts for dry reforming of methane. *Green Chem.* **2014**, *2*, 885–896.

8. Dimitriou, I.; Garcia-Gutierrez, P.; Elder, R.H.; Cueller-Franca, R.M.; Azapagic, A.; Allen, R.W.K. Carbon dioxide utilisation for production of transport fuel: process and economic analysis. *Energ. Environ. Sci.*, **2015** , *8*, 1775-1789

9. Affar, M.M.; Nahil, M.A.; Williams, P.T. Parametric study of CO_2 methanation for synthetic natural gas production. *Energy Technol*. **2019**, 7, 190075.

10. Aziz, M.A.A.; Jalil, A.A.; Triwahyono, S.; Sidik, S.M. Methanation of carbon dioxide on metal-promoted mesostructured silica nanoparticles. *Appl. Catal. A* **2014**, *486*, 115–122.

11. Frontera, P.; Macario, A.; Ferraro, M.; Antonucci, P.L.; Supported Catalysts for CO2 Methanation: A Review, catalyst **2017**,7,59,1-28

12. Daroughegi, R.; Meshjani, F.; Rezaei, M. Enhanced activity of CO_2 methanation over mesoporous nanocrystalline Ni-Al_2O_3 catalysts prepared by ultrasound-assisted co-precipitation method. *Int. J. Hydrogen Energy* **2017**, 42, 15115–15125.

13. Cho, E.H.; Kim, W.H.; Ko, C.H.; Yoon, W.L. Enhanced CO_2 methanation reaction in C1 chemistry over a highly dispersed nickel nanocatalyst prepared using the one-step melt-infiltration method. *Catalysts* **2020**, *10*, 643.

14. Aziz, M.A.A.; Jali, A.A.; Triwahyono, S.; Saad, M.W.A. CO_2 methanation over Ni-promoted mesostructured silica nanoparticles: Influence of Ni loading and water vapor on activity and response surface methodology studies. *Chem. Eng. J.* **2015**, *260*, 757–764.

15. Vertivel, S.; Stefan, N.; Ralf, Z.; Helmut, P.; Gunther, K. Effect of support and chelating ligand on the synthesis of Ni catalysts with high activity and stability for CO_2 methanation. *Catalysts* **2020**, *10*, 493.

16. L. Wang, J. Hu, H. Liu, Q. Wei, D. Gong, L. Mo, H. Tao, C. Zhang, Three-Dimensional Mesoporous Ni-CeO_2 Catalysts with Ni Embedded in the Pore Walls for CO_2 Methanation, *catalysts*, 2020, *10*, 523

17. Hu, D.; Gao, J.; Ping Y, Jia, L.; Gunawan, P.; Gu, Fanga.; Su, Fabing. Enhanced investigation of CO methanation over Ni/Al2O3 for synthetic natural gas production. *Ind. Eng. Chem. Res.*, **2012**, 51, 4875-86

18. Fan M-T, Miao K-P, Lin J-D et al, Mg-Al oxide supported Ni catalysts with enhanced stability for efficient synthetic natural gas from syngas, *Appl. Surf Sci.*, 2014, 307, 682-8

19. J. Tan, J. Wang, Z. Zhang, Z. Ma, L. Wang, Y. Liu, Highly dispersed and stable Ni nanoparticles confined by MgO on ZrO_2 for CO_2 methanation, *Appl. Surface science*, 2019, *281*, 1538-1548

20. Yan, Y.; Dai, Y.; He, H.; Yu, Y.; Yang, Y. A novel W-doped Ni-Mg mixed oxide catalyst for CO2 methanation, *Appl. Catal.* **2016**, *196* 108-116

21. Lin, J.; Ma, C.; Wang, Q.; Xu, Y.; Ma, G.; Wang, J.; Wang, H,; Dong, C.; Zhang, C.; Ding, M. Enhanced low-temperature performance of CO_2 methanation over mesoporous Ni/Al_2O_3-ZrO_2 catalysts. *Appl. Catal. B* **2019**, *243*, 262–272.

22. Petala, A.; Panagiotoppuluo, P. Methanation of CO_2 over alkali-promoted Ru/TiO_2 catalysts: I. Effect of alkali additives on catalytic activity and selectivity. *Appl. Catal. B* **2018**, *224*, 919–927.

23. Guo, M.; Lu, G. The effect of impregnation strategy on structural characters and CO_2 methanation properties over MgO modified Ni/SiO_2 catalysts. *Cat. Commun.* **2014**, *54*, 55–60.

24. Thien A.L.; Jieum K;. Eun Duck Park.; CO and CO2 methanation over M(=Mn,Ce,Zr,Mg,K,Zn, or V)-promoted Ni/Al@Al2O3 catalysts. *Catalysis Today* **2020,** *348*, 88-88.

25. Bette, N.; Thielemann, J.; Schreiner, M.; Mertens, F. Methanation of CO_2 over a (Mg, Al)O$_x$ supported nickel catalyst derived from a Ni, Mg, Al-hydrotalcite-like precursor. *ChemCatChem* **2016**, *8*, 2903.

26. Duyar, M.S.; Wang, S.; Arellano-Trevirio, M.A.; Farrauto, R.J. CO_2 utilization with a novel dual function material (DFM) for capture and catalytic conversion to synthetic natural gas: An update. *J. CO2 Util.* **2016**, *15*, 65–71.

27. Fisher, J.C.; Siriwardane, R.V. $Mg(OH)_2$ for CO_2 capture from high-pressure, moderate-temperature gas streams. *Energy Fuels* **2014**, *28*, 5936–5941.

28. Loder, A.; Siebenhofer, M.; Lux, S. The reaction kinetics of CO_2 methanation on a bifunctional Ni/MgO catalyst. *J. Ind. Eng. Chem.* **2020**, *85*, 196–207.

29. Jia, X.; Zhang, X.; Rui, N.; Hu, X.; Chang-jun, L. Structural effect of Ni/ZrO_2 catalyst on CO_2 methanation with enhanced activity. *Appl. Catal. B* **2019**, *244*, 159–169.

30. Carbarino, G.; Riani, P.; Magistri, L.; Busca, G. A study of the methanation of carbon dioxide on Ni/Al_2O_3 catalysts at atmospheric pressure. *Int. J. Hydrogen Energy* **2014**, *39*, 11557–11565.

31. Marocco, P.; Morosanu, E.A.; Giglio, E.; Ferrero, D.; Mebrahtu, C.; Lanzini, A.; Abate, S.; Bensaid, S.; Perathoner, S.; Santarelli, M.; Piroone, R.; Centi, G. CO_2 methanation Ni/Al hydrotalcite-derived catalyst: Experimental characterization and kinetic study. *Fuel* **2018**, *225*, 230–242.

32. Muroyama, H.; Tsuda, Y.; Asakoshi, T.; Masitah, H.; Okanishi, T.; Matsui, T.; Eguchi, K. Carbon dioxide methanation over Ni catalysts supported on various metal oxides. *J of Catalysis* **2016,** *343*, 178-184

33. A. Zhao, W. ying, H. Zhang, H. Ma, D. Fang, Ni–Al2O3 catalysts prepared by solution combustion method for syngas methanation, *Catalysis Communications*, 2012, 17, 34-38

34. Tada, S.; Shimizu, T,; Kameyama, H,; Haneda, T, Ni/CeO2 catalysts with high CO_2 methanation activity and high CH4 selectivity at low temperature, *Int' J. of hydrogen energy* 37(2012) 5527-5531

35. Song, F.; Zhong, Q.; Yu, Y.;   Shi, M.; Wu, Y.; Hu, J; Song, Y.; Obtaining well-dispersed Ni/Al_2O_3 catalyst for CO2 methanation with a microwave-assisted method, *Int. J. of Hydrogen Energy* **2**017, 174-4183

36. Pradita, T.; Shih, S.J.; Aji, B.B.; Sudibyo. Synthesis of MgO powder from magnesium nitrate using spray pyrolysis. *AIP Conf. Proc.* **2017**, *1823*, 020016.

37 G. Jiajian, Y. Wang, Y. Ping, Y. Ping, F. Su, A thermodynamic analysis of methanation reactions of carbon oxides for the production of synthetic natural gas, RSC Advanced, 2012, 2, 2358-2368

38. Rahmani, S.; Rezaei, M.; Meshkani, F. Preparation of highly active nickel catalysts supported on mesoporous nanocrystalline Al_2O_3 for CO_2 methanation. *J. Ind. Eng. Chem.* **2014**, 20, 1346–1352.

39 . Aziz, A.A.A.; Jalil, A.A.; Triwahyono, S.; Mukti, R.; Taufiq-Yap, Y.H.; Sazegar, M.R. Highly active Ni-promoted mesostructured silica nanoparticles for CO_2 methanation. *Appl. Catal. B* **2014**, *147*, 359–368.

40. Abate, S.; Barbera, K.; Giglio, E.; Deorsola, F.; Bensaid, S.; Perathoner, S.; Pirone, R.; Centi, G. Synthesis, Characterization, and activity pattern of Ni-Al Hydrotalcite catalysts in CO_2 methanation. *Ind. Eng. Chem. Res.* **2016**, *55*, 8299–8308.

41. Jugensen, L.; Ehimen, E.A.; Born, J.; Hole-Nielsen, J.B. Dynamic biogas upgrading based on the Sabatier process: Thermodynamic and dynamic process simulation. *Bioresource Technol*. **2015**, *178*, 323–329.